J Electr Eng Technol.2018; 13(2): 752-760
http://doi.org/10.5370/JEET.2018.13.2.752

ISSN(Print) 1975-0102
ISSN(Online) 2093-7423

IPMSM Design for Sensorless Control Considering Magnetic Neutral Point Shift According to Magnetic Saturation

JaeWan Choi,* Hyun-Soo Seol* and Ju Lee†

Abstract – In this paper, interior permanent magnet synchronous motor (IPMSM) design for sensorless drive, considering magnetic neutral point shift according to magnetic saturation, has been proposed. Sensorless control was divided into a method based on inductance and a method based on back induced voltage. Because induced voltage is very small at zero or low speed, error in rotor initial position estimation may occur. Using the ratio of saliency addresses this problem. When using high-frequency injections at low speed, the rotor's initial position is estimated at the smallest portion of the inductance. IPMSM has the minimum inductance at the d-axis. However, if magnetic saturation leads to magnetic neutral point variation, following the load current change, there is a change in the minimum point of inductance. In this case, it can lead to failure of initial rotor position estimation. As a result, it is essential that the blocking design has an inductance minimum point shift. As such, in this study, an IPMSM design method, by blocking magnetic neutral point change, has been proposed. After determining the inductance profile based on the finite element analysis (FEA), the results of proposed method were verified.

Keywords: Inductance profile, IPMSM design method, Loading distribution method, Magnetic saturation, Saliency, Sensorless control

1. Introduction

Interior permanent magnet synchronous motor(IPMSM) is an electric motor that is used in many industrial fields owing to its wide range of operating areas and high output density [1-15]. IPMSM is primarily driven by vector control, that requires precise position of the rotor. Thus, a position sensor such as encoder and resolver is attached to the axial direction to estimate the correct rotor position. Unfortunately, this leads to an increase in the cost of production and required motor size [5-8].

Within this context, small and lightweight automotive motors are the primary topic, because weight increase leads to fuel loss and degradation in output. Therefore, with the adoption of the sensorless control method, it is possible to resolve the aforementioned issues [1].

Sensorless control is divided into two method: one based on inductance and another one based on back induced voltage. Because induced voltage is very small from zero to low speed, high-frequency voltage injections, based on inductance, are mainly used [1-4]. IPMSM has the minimal inductance at the d-axis. However, if magnetic saturation leads to magnetic neutral point variation, following the load current change, there is a change in the minimum point of inductance. In this case, it can lead to failure of initial rotor position estimation. Thus, in this study, the motor design for sensorless control takes into account the magnetic saturation characteristics of IPMSM [13-17].

† Corresponding Author: Dept. of Electrical Engineering, Hanyang University, Korea. (julee@hanyang.ac.kr)
* Dept. of Electrical Engineering, Hanyang University, Korea. ({cartn, mookhang16}@naver.com)
Received: June 23, 2017; Accepted: November 8, 2017

2. Sensorless Control Based on Inductance

For sensorless control based on inductance, inject a high-frequency voltage of (1) in the current controller output portion as illustrated, Fig. 1 [1-4].

$$V_{dsh}^{r} = \cos\omega_h t \ , \ V_{dsh}^{r} = 0 \tag{1}$$

Arranging the equation of the injected high-frequency voltage and the associated high-frequency currents obtains (2).

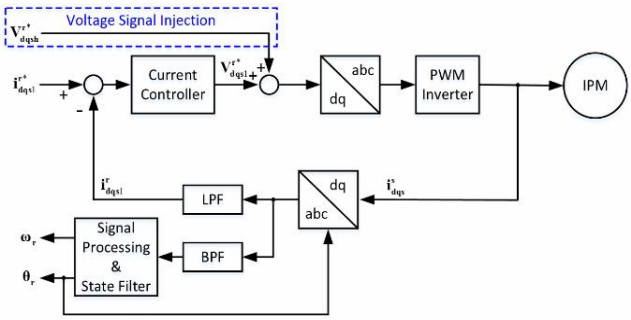

Fig. 1. Sensorless control block diagram

$$\begin{bmatrix} i_{dsh}^{s} \\ i_{qsh}^{s} \end{bmatrix} = \begin{bmatrix} \dfrac{1}{L_{dh}^{r} \cdot \omega_h} \cos(\theta_r) \sin \omega_h t \\ \dfrac{1}{L_{dh}^{r} \cdot \omega_h} \sin(\theta_r) \sin \omega_h t \end{bmatrix} \tag{2}$$

As indicated by (2), the current signal contains information of each angle and frequency component of the rotor. The rotor position is determined from the current signal by removing the frequency component from this equation. This means that the inductance components involved in the expression are important parameters for the estimation of the rotor position [18].

3. IPMSM Initial Model

The initial model was chosen for ISG (Idel & Go) motors for 10kW vehicles. As mentioned above, the motor of the vehicle is suitable for sensorless control considering light weight and lightening trend. Based on the specifications of Table 1, the initial model of Fig. 2 was designed.

3.1 IPMSM initial model FEA result

The flux line of the initial model as illustrated is Fig. 3. Unlike the no Load state in the Fig. 3(a), the armature reaction results in the movement of the magnetic neutral point when in a loaded state, causing the inductance variation [16].

The inductance profile for the initial model is depicted in Fig. 4. The larger the variation in the load current, the larger the changes in the inductance profile. Ultimately, when the rated current (175A) was applied, the inductance profile shifted to a 72.48 [°E]. Additionally, the minimum point of inductance was shifted [14-17].

IPMSM is an electric motor that uses both magnetic torque and reluctance torque. To achieve maximum output control, command the current vector of the two quadrants [15-17].

However, if the inductance profile is changed, such as with the initial model, it will not generate maximum Torque from sensorless vector controls based on the

Table 1. Specification of initial model

Parameter	Value	Unit
Pole / Slot	8 / 48	-
Stator / Rotor Outer Diameter	147 / 70	mm
Stack Length	46	mm
Rated Speed / Torque	2000 / 12.20	rpm / Nm
Max Speed / Torque	16000 / 1.4	rpm / Nm
Voltage Limit	60	V_{dc}
Current Density Limit	8	A/mm^2
Core Type	35PN230	-
Permanent Magnet	NdFeB (B_r=1.19T)	-

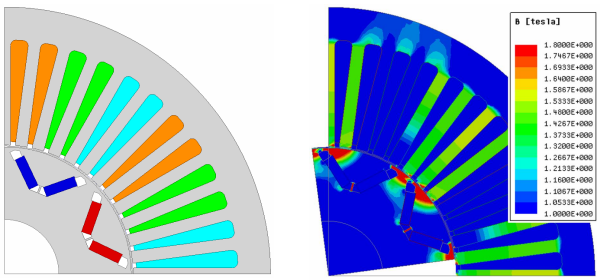

(a) Initial Model (b) B Field

Fig. 2. Initial model of IPMSM for sensorless control

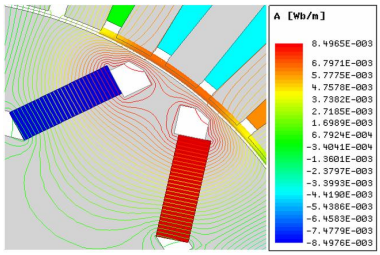

(a) No Load

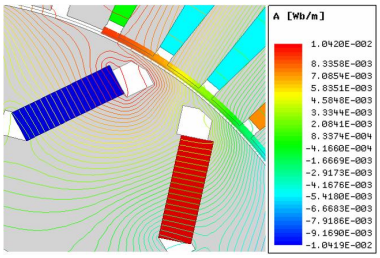

(b) Rated Load (175A, 32°)

Fig. 3. Flux line of initial model

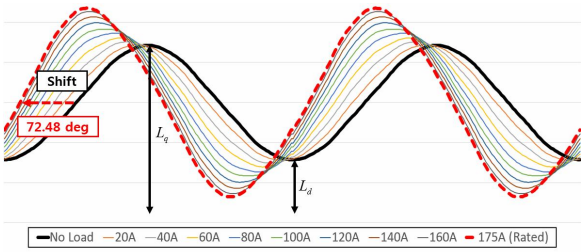

Fig. 4. Inductance profile of initial model (at 2000rpm)

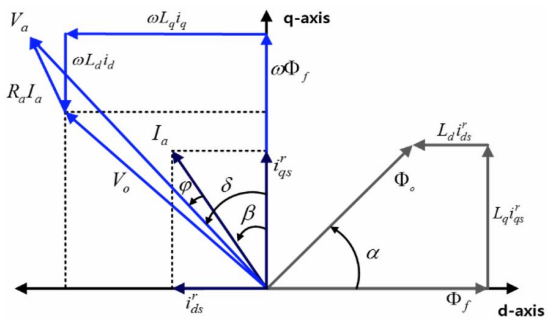

Fig. 5. IPMSM vector diagram

inductance. In the worst case, if the inductance profile variation is greater than 90 [°E] [4], it causes a command of the three current vector command. This then, causes it to operate with a generator rather than a motor. As a result, the sensorless control motor requires a design that minimizes the inductance profile variation [17].

4. Loading Distribution Method

4.1 Definition of Loading

(3) is the total magnetic loading. (4) is the magnetic loading. p is half of the number of poles. ϕ_g is the average air gap flux per pole.

$$\text{Total magnetic loading} = 2p\phi \tag{3}$$

$$B_{gav} = \frac{2p\phi_g}{\pi D_g L_{stk}} \text{ [T]} \tag{4}$$

(5) is the total electric loading. (6) is the electric loading.

$$\text{Total electric loading} = I_a Z \text{ [Ampere Conductor]} \tag{5}$$

$$ac = \frac{I_a Z}{\pi D_g} \text{ [Ampere Conductor / m]} \tag{6}$$

4.2 Torque equation of IPMSM

The IPMSM torque equation is expressed by separating magnetic torque(T_m) and reluctance torque(T_r) (7)

$$T = \frac{3}{2} p\lambda_{pm} I_a \cos\theta + \frac{3}{4} p(L_d - L_q) I_a^2 \sin 2\beta \;=\; T_m + T_L \tag{7}$$

The above equation is expressed in (8), including the previously mentioned the magnetic loading and the electric loading.

$$T = \frac{\pi}{4} k_w B_{g1} ac D_g^2 L_{stk} \tag{8}$$

Finally, the torque equation can be expressed as a product of the magnetic loading and the electric loading [19].

5. IPMSM Design Considering Magnetic Neutral Point Variation

5.1 Determination of design parameters (Step 1)

In the previous chapter, the inductance variation was considered to be an effect of the armature reaction. The armature reaction increases proportionally to the magnitude of the current. Thus, inductance variation becomes larger depending on the increase in the current magnitude. In other words, it was determined that the inductance variation was very closely related to electrical loading.

As a result, the object function of the improvement design was determined by reducing the electric loading and increasing the magnetic loading.

The external diameter of the rotor and the use of a permanent magnet were selected to increase the magnetic loading. Additionally, the mount of total conductor and magnitude of the stator current were selected to reduce the electric loading. Based on the selected design variables, the process of Fig. 6 was proceeded.

- Maximize Magnetic Loading : $f_{ml}(x_1, x_2, x_3, x_4)$
- Minimize Electric Loading : $f_{el}(x_1, x_2, x_3, x_4)$
- Usage of Magnet : x_1
- the number of Stator Turns : x_2
- Stator Current : x_3
- Rotor Outer Diameter : x_4
- Maximize Output Torque : $g_t(x_1, x_2, x_3, x_4)$
- Inductance Variation : $g_{iv}(x_1, x_2, x_3, x_4)$

Objective functions

$f_{ml}(x_1, x_2, x_3, x_4) + f_{el}(x_1, x_2, x_3, x_4)$

Constraint conditions

$g_t(x_1, x_2, x_3, x_4) \geq 12.20$

$g_t(x_1, x_2, x_3, x_4) \leq 25$

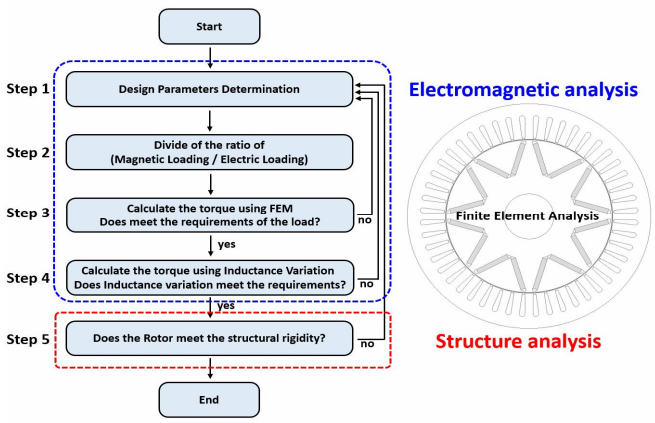

Fig. 6. Improved model design block diagram

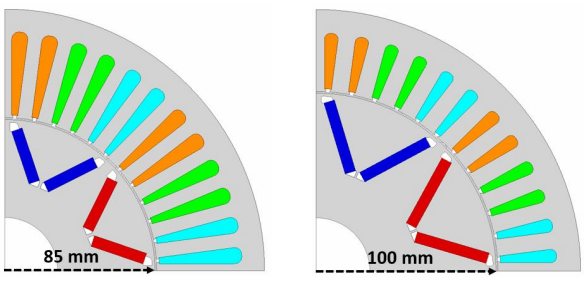

(a) Model 1 (b) Model 2

Fig. 7. Improved model

Table 2. Specification of improved model

		model		
		initial	#1	#2
Rotor Diameter [mm]		175	170	200
Usage of Magnet [mm^2]		97.2	192.2	249.0
Stator Turns		6	4	3
Rated Current [A_{rms}]		175	185	195
Torque [Nm]	2000rpm	12.92	12.83	12.51
	16000rpm	4.08	3.65	1.72

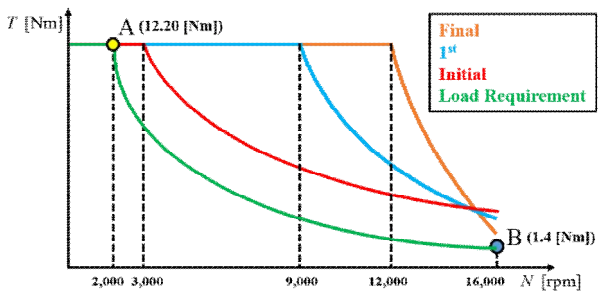

Fig. 8. Speed-Torque Graph of each model

5.2 Design based on loading distribution method (Step 2)

The size of the rotor and stator were determined based on a loading distribution method under conditions of generating identical torque. The improvement model and detailed specifications are shown in Fig. 7 and Table 2 respectively.

The load requirement and speed-torque graph of each model are shown in Fig.8. Under the same output, the higher the magnetic loading, the lower the field weakening control region [20]. Considering these characteristics, the improved model design was leveraged to meet the requirements of the load at the highest speed.

5.3 Check of constraint conditions (Step 3, 4)

The magnetic and electric loading of the improved model are shown in Table 3. The inductance profile of the improved model is illustrated in Fig. 8. Based on this, the correlation between the ratio of loading and inductance variation was analyzed.

Table 3 and Fig. 8 illustrate that, by reducing the electric loading and increasing the magnetic loading, the inductance variation decreases.

The magnetic & electric loading of improved model are shown in Table 3. The inductance profile of the improved model is shown in Fig. 8.

As shown in Fig.10, decreasing the electrical loading reduces the effect of the armature reaction. This means that an increase to the magnetic loading is key to improving the model design. However, increasing the usage of the permanent magnets, to increase the magnetic loading, may result in a rise in production costs. Therefore, the next chapter will select various design variables of the stator and rotor, except the permanent magnet, and identify factors influencing inductance variation.

Table 3. Specification of improved model

	Model		
	Initial	#1	#2
Electric Loading [A/m]	114591.6	83135.1	44690.7
Magnetic Loading [T]	0.5054	0.7317	0.8034
Inductance Variation [°E]	72.48	41.47	25.63

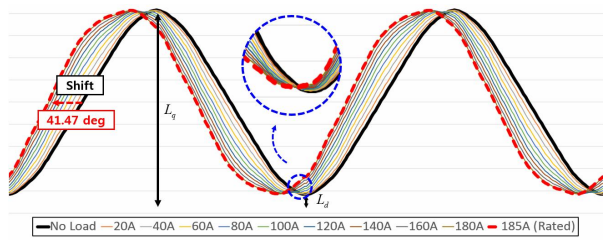

(a) Model 1

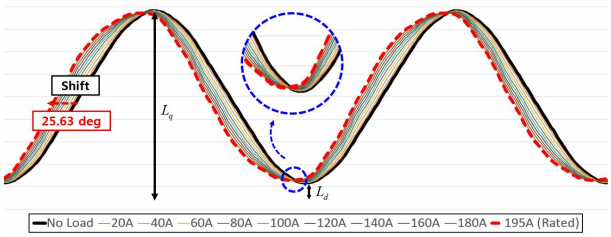

(b) Model 2

Fig. 9. Inductance profile of improved model (at 2000rpm)

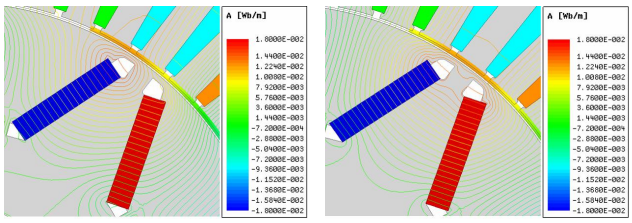

(a) No Load (Model 1) (b) Rated Load (Model 1)

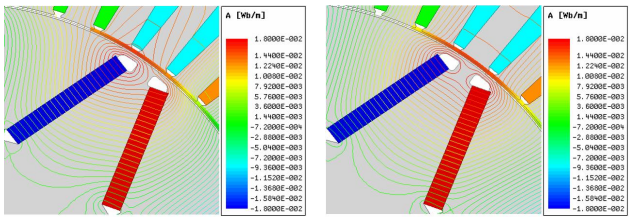

(c) No Load (Model 2) (d) Rated Load (Model 2)

Fig. 10. Flux line of the improved model

5.4 Determination of additional design parameters (Step 1)

As many design variables selection are considered to be more accurate. As such, it is desirable to select as many

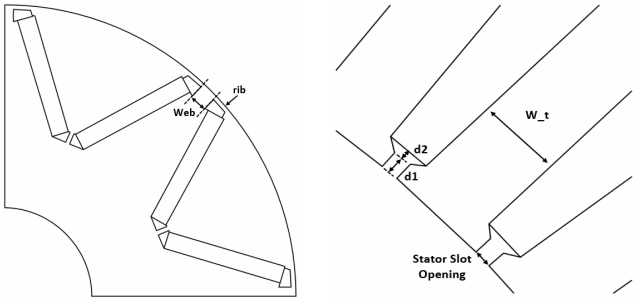

(a) Rotor (b) Stator

Fig 11. Nomenclature of each parts

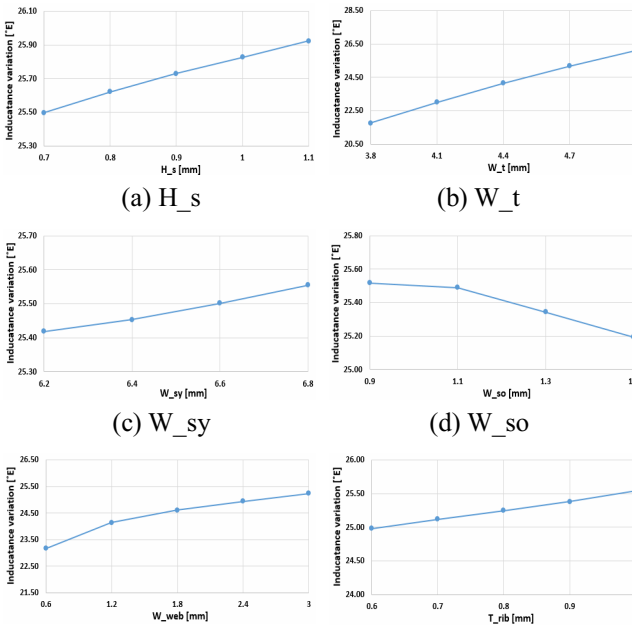

(a) H_s (b) W_t

(c) W_sy (d) W_so

(e) W_web (f) T_rib

Fig. 12. Effects of each design variable (inductance variation)

design variables as possible. However, since the increase in design variables requires an increased number of simulations, it is necessary to select the proper set of variables. In this study, the four design variables that were considered in the preceding paragraph were identical to model 2. The six variables described in Fig. 11 were further selected and analyzed.

The primary intent of the design was to reduce the inductance variation. The constraint conditions of design were torque, torque ripple and efficiency. Based on these conditions, a simulation was performed and the result was analyzed.

In this study, the primary objective is to reduce the inductance variation. However, if torque and efficiency are disregarded, the motor performance is adversely affected. Therefore, the design parameters were selected in consideration of torque, torque ripple and efficiency under conditions that minimize inductance variation.

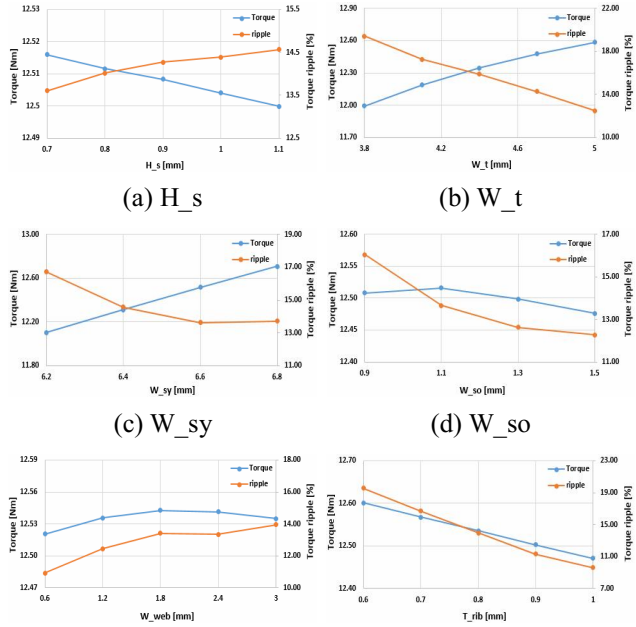

(a) H_s (b) W_t

(c) W_sy (d) W_so

(e) W_web (f) T_rib

Fig. 13. Effects of each design variable (torque and ripple)

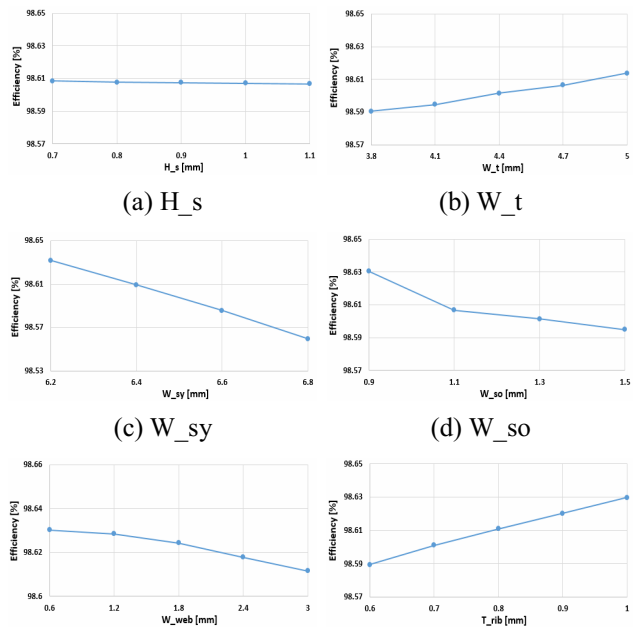

(a) H_s (b) W_t

(c) W_sy (d) W_so

(e) W_web (f) T_rib

Fig. 14. Effects of each design variable (efficiency)

5.5 Analysis based on various design parameters

From now on, the effect of each design parameters on the object function and constraint conditions will be covered. As illustrated by Fig. 15, the aspect of magnetic saturation varies de-pending on the variation in design variables. The variation in magnetic flux characteristics of the motor core has a significant effect on the magnetic field characteristics.

As a result, the object function and constraint condition will be reviewed, and the final model will be designed considering the effects on magnetic saturation.

(For stator parameters)

First, if the thickness of teeth becomes thinner, it becomes more prone to saturation. Hence, inductance variation was decreased. Additionally, output and efficiency tended to decrease, and torque ripple tended to increase. Finally, it was chosen as 5 mm with the overall consideration.

Second, the smaller the height of the shoe, the wider the region of magnetic saturation field. Inductance variation tended to decrease. There was little change in efficiency, and the height of the shoe was selected as 0.7 mm considering the reduction of torque ripple.

Third, the smaller the width of slot, the greater the inductan-ce variation; efficiency, output and torque ripple tended to increase. However, if it was too small, it led to difficulty in inserting the windings and insulators. So, it was chosen as 1.5 mm.

Fourth, the lesser the thickness of the stator yoke, the smaller the inductance variation. Additionally, as output decreased, the efficiency and torque ripple tended to increase. For this consideration, it was chosen as 6.5 mm.

In conclusion, the stator design parameters demonstrated that the wider the range of magnetic saturation fields, the smaller the inductance variation.

(For rotor parameters)

First, the thinner the thickness of web, the smaller the inductance variation. Torque ripple tended to decrease, as efficiency increased. As the web became thinner, most of the electromagnetic field characteristics considered in this study were excellent. However, if it is too thin, it is difficult to maintain the mechanical strength during prolonged periods of rotation at high speed. For this consideration, it was chosen as 0.6 mm.

Second, if the thickness of rib became thinner, it became more prone to saturation. Hence, inductance variation decreased. Both output and torque ripples tended to increase. However, as with the web, there is a possibility that stress was concentrated on the ribs at a high speed rotation. For this consideration, it was chosen as 0.7 mm.

In conclusion, the magnetic saturation of core and inductance changes are closely related. In particular, the width of teeth and web are large contributors to inductance variation because of the design flexibility. Based upon the rotor design parameter, the width of rib and web, it is necessary to select parameters considering the structural rigidity. This is owed to the possibility that rotor deformation can occur at high speed rotation.

Table 4. Design parameter of final model

Variable		Model 2	Final Model
Stator	Height of shoe	0.8 mm	0.7 mm (↓)
	Width of teeth	4.8 mm	5.0 mm (↑)
	Width of back yoke	6.6 mm	6.3 mm (↓)
	Slot opening	1.1 mm	1.2 mm (↑)
Rotor	Width of web	3.0 mm	0.6 mm (↓)
	Thickness of rib	0.8 mm	0.7 mm (↓)

5.6 Performance of Final Model (Step 3, 4)

The design variables selected through the optimized process are shown in Table 4. The performance of the final

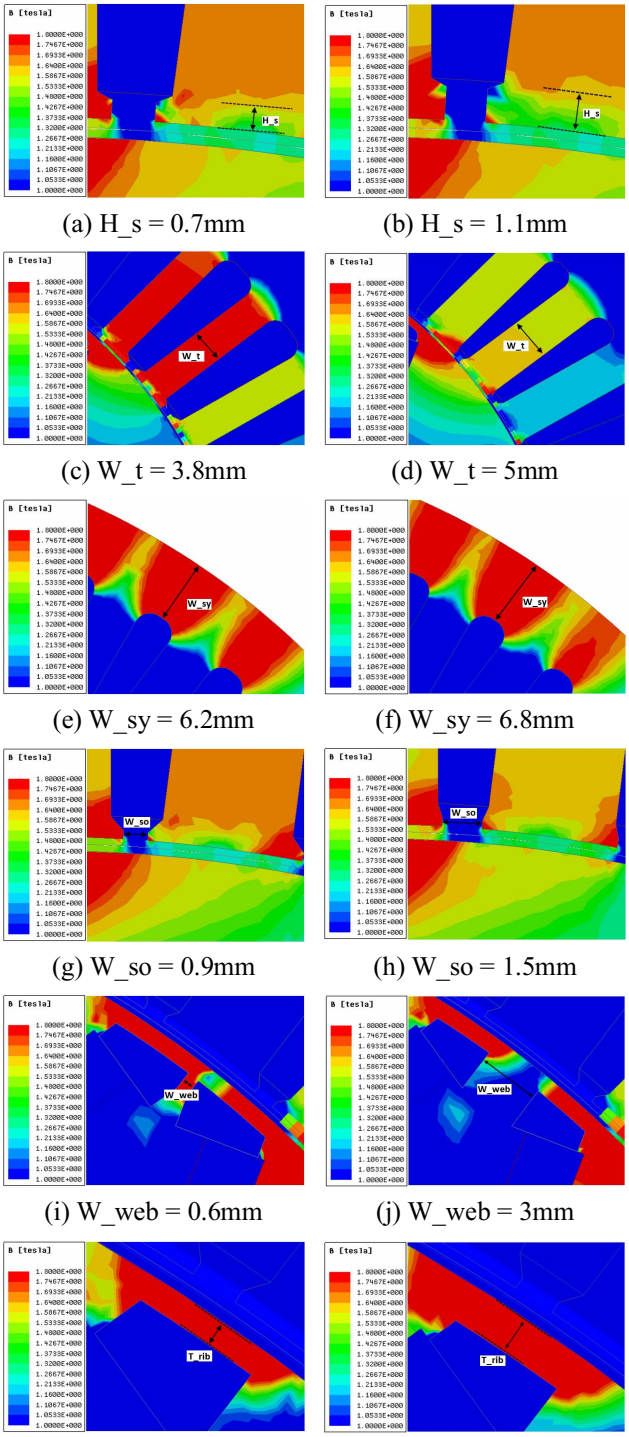

(a) H_s = 0.7mm (b) H_s = 1.1mm

(c) W_t = 3.8mm (d) W_t = 5mm

(e) W_sy = 6.2mm (f) W_sy = 6.8mm

(g) W_so = 0.9mm (h) W_so = 1.5mm

(i) W_web = 0.6mm (j) W_web = 3mm

(k) T_rib = 0.6mm (l) T_rib = 1mm

Fig. 15. B Field depending on each part variation

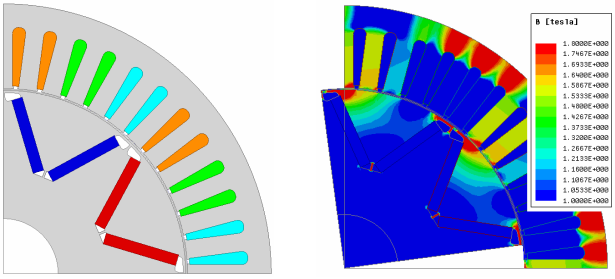

(a) Final Model (b) B Field

Fig. 16. Final model of IPMSM for sensorless control

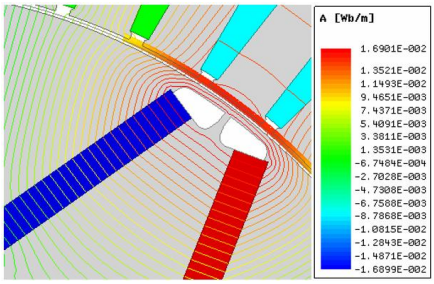

(a) No Load

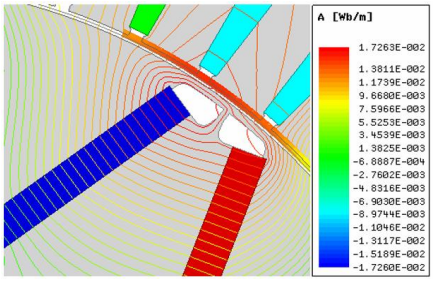

(b) Rated Load (195A, 18deg)

Fig. 17. Flux line of final model

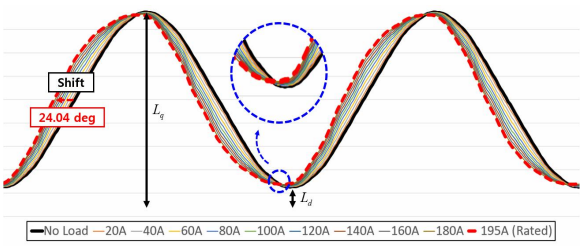

Fig. 18. Inductance profile of final model (at 2,000rpm)

model is depicted in Table Fig. 16 and Table 5, respectively.

Compared to the initial model, at a rated speed of 2,000 rpm, the inductance variation decreased approximately 48 [°E] and efficiency increased by approximately 1 [%]. At the highest speed, both torque and efficiency were reduced. Because the final model had a higher the magnetic loading, the field weakening control region was shorten. The efficiency was reduced by 5 [%] owing to the increase in core loss. Eddy current loss was greater than the decrease in cooper loss.

Table 6. Inductance of initial & final model

		Model	
		Initial	Final
2,000 [rpm] (Rated)	Ld [mH]	0.0479	0.0056
	Lq [mH]	0.0927	0.0114
	The ratio of Inductance (Lq / Ld)	1.93	2.03
16,000 [rpm] (Maximum)	Ld [mH]	0.0526	0.0042
	Lq [mH]	0.1232	0.0145
	The ratio of Inductance (Lq / Ld)	2.34	3.45

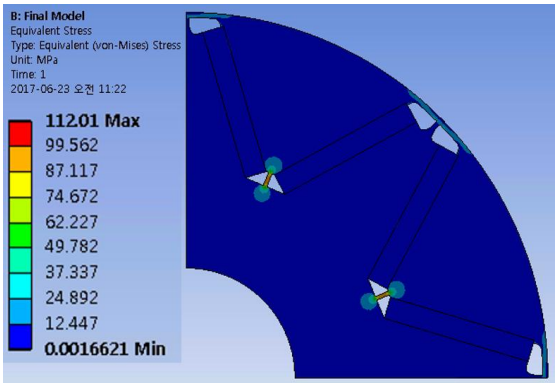

Fig. 19. Stiffness analysis of final model

Fig. 17 represents the flux line of the final model. There is no appreciable difference between the no load and rated load condition. In other words, the magnetic neutral point shift, according to load conditions, is small. As such, inductance variation in Fig. 18 was decreased. This means that the final model is suitable for the sensorless control motor.

The inductance of the initial and final models are shown in Table 6. Saliency is very important in sensorless control based on inductance [21]. The final model has a higher saliency compared to the initial model at rated / maximum speed. Therefore, the final model is better suited for sensorless control.

5.7 Check of Structural Rigidity (Step 5)

The analysis results of the final design are illustrated in Fig. 19. Tensile force is defined as the force that a permanent magnet tries to bounce out. Additionally, tensile strength is defined as a force that prevents the scattering of permanent magnets. Finally, the safety coefficient is defined as the maximum tensile strength divided by the maximum stress.

$$k_{safe} = \frac{Yidle\ Strentgh}{Equivalent\ stress} = \frac{2.5\times10^2}{112.01} = 2.23 \qquad (9)$$

The safety coefficient indicates that the structural safety standards (1.5) are met.

6. Conclusion

In this paper, the design of synchronous motor designs for sensorless control was analyzed. As noted above, the typical motor increases inductance phase angle differences as the load current increases. As such, maximum output control cannot be achieved when sensorless vector control is based on inductance. To improve this, reducing the electric loading, under the same torque generating condition s, is a key design point. In addition, a parametric analysis of IPMSM elements was conducted in order to identify the correlation between the magnetic saturation phase change and inductance phase change. In conclusion, it is necessary to design both magnetic saturation and structural rigidity simultaneously. The results analyzed in this paper will be useful research material for the design of motor vehicles for sensorless control.

Acknowledgements

This work was supported by the Human Resources Program in Energy Technology of the Korea Institute of Energy Technology Evaluation and Planning (KETEP) under grant (20154030200900), and the National Research Foundation of Korea(NRF) grant funded by the Korea government(Ministry of Science, ICT & Future Planning) (No. 2016R1A2A1A05005392).

References

[1] Myung-Seop Lim, Seung-Hee Chai and Jung-Pyo Hong, "Design of Saliency-Based Sensorless-Controlled IPMSM With Concentrated Winding for EV Traction," *IEEE Transactions on Magnetics,* vol. 52, no. 3, March 2016.

[2] Sang-Il Kim; Jun-Hyuk Im; Eui-Young Song; Rae-Young Kim, "A New Rotor Position Estimation Method of IPMSM Using All-Pass Filter on High-Frequency Rotating Voltage Signal Injection," *IEEE Transactions on Industrial Electronics,* vol. 63, no. 10, pp.6499-6509, July 2016.

[3] Yong-Cheol Kwon, Seung-Ki Sul, Noor Aamir Baloch, Shinya Morimoto and Motomichi Ohto, "Design, Modeling, and Control of an IPMSM With an Asymmetric Rotor and Search Coils for Absolute Position Sensorless Drive," *IEEE Transactions on Industry Applications,* vol. 52, no. 5, pp. 3839-3850, October 2016.

[4] Yingguang Sun, Matthias Preindl, Shahin Sirouspour and Ali Emadi, "Unified Wide-Speed Sensorless Scheme Using Nonlinear Optimization for IPMSM Drives," *IEEE Transactions on Power Electronics,* vol. 32, no. 8, pp. 6308-6322, October 2016.

[5] Nobuyuki Imai, Shigeo Morimoto, Masayuki Sanada and Yoji Takeda, "Influence of Rotor Configuration on Sensorless Control for Permanent-Magnet Synchronous Motors," *IEEE Transactions on Industry Applications,* vol. 44, no. 1, pp. 93-100, January 2008.

[6] Amor Khlaief, Moussa Bendjedia, Mohamed Boussak and Moncef Gossa, "A Nonlinear Observer for High-Performance Sensorless Speed Control of IPMSM Drive," *IEEE Transactions on Power Electronics*, vol. 27, no. 6, pp. 3028-3040, November 2011.

[7] Zhuangyao Tang; Xiong Li, Serkan Dusmez and Bilal Akin, "A New V-f-Based Sensorless MTPA Control for IPMSM Drives," *IEEE Transactions on Power Electronics*, vol. 31, no. 6, pp. 4400-4415, August 2016.

[8] Sang-Il Kim, Jun-Hyuk Im, Eui-Young Song and Rae-Young Kim, "A New Rotor Position Estimation Method of IPMSM Using All-Pass Filter on High-Frequency Rotating Voltage Signal Injection," *IEEE Transactions on Industrial Electronics,* vol. 63, no. 10, pp. 6499-6509, July. 2016.

[9] S. Ostlund and M. Brokemper, "Sensorless rotor-position detection from zero to rated speed for an integrated PM synchronous motor drive," *IEEE Transactions on Industry Applications*, vol. 32, no. 5, pp. 1158-1165, October 1996.

[10] Luca Rovere, Andrea Formentini, Alberto Gaeta, Pericle Zanchetta and Mario Marchesoni, "Sensorless Finite-Control Set Model Predictive Control for IPMSM Drives," *IEEE Transactions on Industrial Electronics,* vol.63, no.9, pp.5921-5931, June 2016.

[11] Gaolin Wang, Lei Yang, Guoqiang Zhang, Xueguang Zhang and Dianguo Xu, "Comparative Investigation of Pseudorandom High-Frequency Signal Injection Schemes for Sensorless IPMSM Drives," *IEEE Transactions on Power Electronics,* vol. 32, no. 3, pp. 2123-2132, May 2016.

[12] M. C. Paicu, I. Boldea, G. -D. Andreescu and F. Blaabjerg "Very low speed performance of active flux based sensorless control interior permanent magnet synchronous motor vector control versus direct torque and flux control," *IET Electric Power Applications,* vol. 3, no. 6, pp. 551-561, November 2009.

[13] Yoshiaki Kano "Torque Ripple Reduction of Saliency-Based Sensorless Drive Concentrated-Winding IPMSM Using Novel Flux Barrier," *IEEE Transactions on Industry Applications,* vol. 51, no. 4, pp. 2905-2916, January 2015.

[14] Yukinori Inoue, Yasunori Kawaguchi, Shigeo Morimoto and Masayuki Sanada "Performance Improvement of Sensorless IPMSM Drives in a Low-Speed Region Using Online Parameter Identification," *IEEE Transactions on Industry Applications,* vol. 47, no. 2, pp. 798-804, December 2010.

[15] Peter Sergeant, Frederik De Belie and Jan Melkebedk "Torque Ripple Reduction of Saliency-Based Sensorless Drive Concentrated-Winding IPMSM

Using Novel Flux Barrier," *IEEE Transactions on Industrial Electronics*, vol. 59, no. 6, pp. 2457-2465, February 2011.

[16] Liu Yue, Pei Yulong, Yu Yanjun, Shi Yanwen and Chai Feng "Increasing the saliency ratio of fractional slot concentrated winding interior permanent magnet synchronous motors," *IET Electric Power Applications*, vol. 9, no. 7, pp. 439-448, July 2015.

[17] S. Morimoto, M. Sanada and Y. Takeda "Mechanical Sensorless Drives of IPMSM With Online Parameter Identification," *IEEE Transactions on Industry Applications*, vol. 42, no. 5, pp. 1241-1248, September 2006.

[18] Young-Doo Yoon, *Electrical Engineering*, "Sensorless Control for AC Machines Based on Square-wave Voltage Injection," *a doctoral* dissertation, *Seoul National University*, 2010.

[19] Jae nam Bae, "Permanent magnet synchronous machine design through an automatic selection of the specific loadings," *a doctoral* dissertation, *Hanyang University*, 2010.

[20] Jung-Min Mun, Gyeong-Jae Park, SangHyeok Seo, Dae-Woo kim, Yong-Jae Kim, Sang-Yong Jung, "Design Characteristics of IPMSM With Wide Constant Power Speed Range for EV Traction," *IEEE Transaction on Magnetics*, vol. 53, no. 6. Feb. 2017.

[21] Jung-Ik Ha, K. Ide, T. Sawa, Seung-Ki Sul, "Sensorless rotor position extimation of an interior permanent magnet motor from initial states," *IEEE Transaction on Industry Applications*, vol. 39, no. 3. May 2003.

JaeWan Choi was born in Busan, Korea, in 1990. He received his B.S degree in Electrical Engineering from Kwang-woon University, Seoul, Korea in 2015. Since 2016, he has been pursuing a M.S degree at the Department of Electrical Engineering, Hanyang University, Seoul, Korea. His research interests include design, analysis, testing and control of motors/generators, power conversion systems and motor drive of electric vehicle.

Hyun-Soo Seol was born in Daegu, Korea, in 1987. He received the B. S. degree in Electronic Information Systems Engineering from Hanyang University, Ansan, Korea, in 2012, and he has been working toward the Ph.D. degree at the Department of Electrical Engineering, Hanyang University, Seoul, Korea. His current research interests include design, analysis, of motor / generator, power conversion systems and home appliances, Automotive Parts.

Ju Lee received the M.S. degree in Electrical Engineering from Hanyang University, Seoul, South Korea, in 1988 and his Ph.D. degree in Electrical Engineering from Kyusyu University, Fukuoka, Japan in 1997. In September 1997, he joined Hanyang University, where he is currently a Professor in the Division of Electrical and Biomedical Engineering. His main research interests include electric machinery and drives, electromagnetic field analysis, transformation systems such as hybrid electric vehicles and high-speed electric trains and standardization. Prof. Lee is a member of the IEEE Industry Applications, IEEE Magnetics, and Power Electronics Society.